JOURNAL OF THE ROYAL SOCIETY Interface

*J. R. Soc. Interface* (2006) **3**, 117–121
doi:10.1098/rsif.2005.0100
*Published online* 29 November 2005

REPORT

# Nano measurements with micro-devices: mechanical properties of hydrated collagen fibrils

**S. J. Eppell[1,†], B. N. Smith[1], H. Kahn[2] and R. Ballarini[3,†]**

[1]*Department of Biomedical Engineering,* [2]*Department of Materials Science and Engineering, and* [3]*Department of Civil Engineering, Case Western Reserve University, Cleveland, OH 44106, USA*

The mechanical response of a biological material to applied forces reflects deformation mechanisms occurring within a hierarchical architecture extending over several distinct length scales. Characterizing and in turn predicting the behaviour of such a material requires an understanding of the mechanical properties of the substructures within the hierarchy, the interaction between the substructures, and the relative influence of each substructure on the overall behaviour. While significant progress has been made in mechanical testing of micrometre to millimetre sized biological specimens, quantitative reproducible experimental techniques for making mechanical measurements on specimens with characteristic dimensions in the smaller range of 10–1000 nm are lacking. Filling this void in experimentation is a necessary step towards the development of realistic multiscale computational models useful to predict and mitigate the risk of bone fracture, design improved synthetic replacements for bones, tendons and ligaments, and engineer bioinspired efficient and environmentally friendly structures. Here, we describe a microelectromechanical systems device for directly measuring the tensile strength, stiffness and fatigue behaviour of nanoscale fibres. We used the device to obtain the first stress–strain curve of an isolated collagen fibril producing the modulus and some fatigue properties of this soft nanofibril.

**Keywords: collagen; microelectromechanical systems; nanostructures; biomechanics; fibril**

## 1. INTRODUCTION

Biological materials are remarkable in that with as little mass as possible they achieve, through judicious arrangements of mundane polymeric and ceramic components, impressive mechanical properties necessary for survival. Be they primarily ceramic (tooth enamel, mollusc shell), polymeric (insect exoskeleton, plant cell walls) or more evenly balanced composites (antler, bone), biological materials are virtually all composites utilizing different proportions of the basic components and a variety of hierarchical structural architectures (Kastelic *et al.* 1978; Baer *et al.* 1987; Lakes 1993; Ashby *et al.* 1995).

While microscopic studies reveal biological composites include as many as five (Kamat *et al.* 2000) or six (Rho *et al.* 1998) distinct substructures (ex. mineral platelets, protein interlayers, collagen fibrils, fibres and lamellae), the influence of these small features in their respective hierarchies on overall mechanical properties is not well understood. This is problematic given that natural materials are assembled from the bottom up utilizing familiar structural control mechanisms such as gene regulation, protein folding and enzyme mediated cross-linking. While laser tweezers (Veigel *et al.* 1998; Mehta *et al.* 1999; Kellermayer *et al.* 2001; Liphardt *et al.* 2001; Fujii *et al.* 2002; Bryant 2003) and atomic force microscopy (AFM) (Clausen-Schaumann *et al.* 2000; Yu 2000; Best *et al.* 2001; Muller 2002) are used to probe structures at the molecular scale, an experimental gap exists between these smallest length scales and the micron and larger scales. Furthermore, laser tweezers are limited to applied loads below *ca* 0.1 nN and AFM has calibration issues associated with specimens that are misaligned with respect to loading axes (Heim *et al.* 2004). If we wish to develop mechanistic models relating global mechanical response to initial assembly steps, then we must develop experimental techniques for measuring the mechanical properties of the smallest substructures. In this report, we demonstrate, by measuring the stress–strain response of a single collagen fibril, that microelectromechanical systems (MEMS) technology offers promise towards filling this gap. While AFM was recently used to measure the response of a single collagen fibril to a monotonically increasing load (Graham *et al.* 2004), our MEMS device allowed the gauge length and diameter of the particular fibril tested to be measured. Thus, the data reported here represents the first stress–strain curve of an isolated collagen fibril both in monotonic and in cyclic loading.

MEMS devices, with dimensions of tens of microns, are ideal platforms for testing mechanical properties of nanoscale structures. We fabricated our MEMS device from a 6 μm film of polycrystalline silicon, as shown in figure 1*a*. It consists of an electrostatic comb-drive actuator shown on the left of the image, fixed and movable pads (labelled 'F' and 'M', respectively) shown on the right of the image across which the fibril is placed, and tether beams (labelled 'T') with dimensions selected to produce the required compliance of the device. Figure 1*b* shows a fibril attached to the pads after a loading experiment was completed. When a voltage is applied across the comb drive, an electrostatic attraction is established (Kahn *et al.* 1999) that causes the central portion of the device, including the movable pad, to move to the left as oriented in figure 1*a*. This generates a pure tensile stress in the fibril and a response that provides the most basic mechanical

[†]Authors for correspondence (sje@case.edu; roberto.ballarini@case.edu).

*Received* 10 August 2005
*Accepted* 7 October 2005

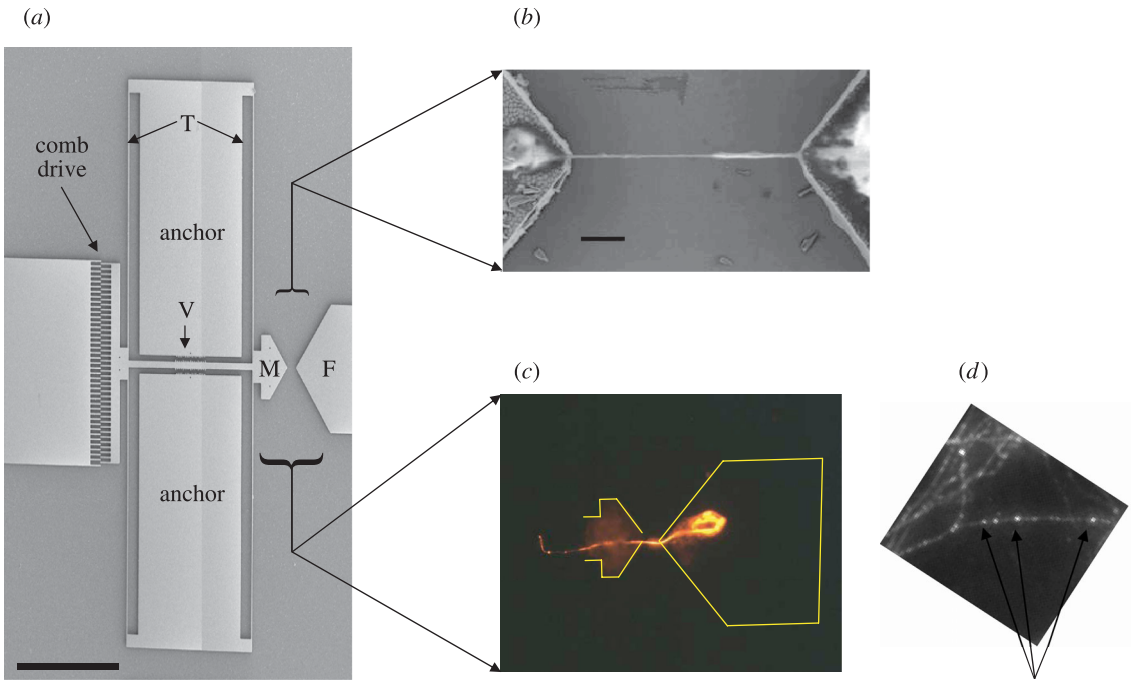


Figure 1. MEMS Mechanical Testing Platform. (*a*) Scanning electron micrograph (SEM) of a polysilicon MEMS device (scale bar, 200 μm). (*b*) Higher magnification SEM showing a fibril attached with epoxy to the two pads. The fibril was loaded in tension and the device stuck at the end of the experiment. Thus, this is an image of a fibril loaded under tension (scale bar, 2 μm). (*c*) Low resolution fluorescent image of a fibril attached across the pads labelled M and F in 1A. Bright outline indicates the device position. (*d*) High resolution fluorescent antibody labelled collagen fibrils (95–350 nm in diameter by SEM) viewed with an optical microscope. While not done in the experiments reported here, the method provides punctate staining of the fibrils (indicated by arrows) that will enable intrinsic strain measurements.

properties, namely axial stiffness and tensile strength. The device displacement is measured using an integrated Vernier scale (labelled V) with 0.25 μm resolution. The force produced by the comb-drive actuator is calibrated by relating the voltage–displacement response of the device loaded with no fibril to the stiffness of the tether beams.[1]

The object used to demonstrate the testing platform is a single type I collagen fibril isolated from the sea cucumber, *Cucumaria frondosa* (Thurmond & Trotter 1996). This nanoscale structure is several dozen microns long, has cross-sectional dimensions *ca* 10–500 nm, and is easily obtainable as an isolated nanofibril. Sea cucumber fibrils are similar to those found in vertebrates having the same length, assembling with the same repeat period, possessing the same gap/overlap ratio (Trotter *et al.* 1994) and possessing the same cross-linking chemistry (Butler *et al.* 1987). The habit of echinoderm fibrils is spindle shaped rather than cylindrical as found in mammals. In addition, the collagen amino and carboxy termini are arranged in a bipolar manner with the centre of symmetry existing at the middle of the long axis of the spindle rather than monopolar as found in mammals. This spindle structure can also be obtained using mammalian collagen monomers to reconstitute synthetic fibrils (Rainey *et al.* 2002). Clear evidence of proteoglycans utilized to aggregate echinoderm fibrils has been found but these molecules are all removed in the purification procedure used to obtain the fibrils we measured (Graham *et al.* 2000). The major difference between Echinoderm collagen fibrils and other animals is at the systemic level (Trotter *et al.* 1994; Thurmond & Trotter 1996). Echinoderms have the ability to change the mechanical properties of their collagen fibrillar networks in a way that is interfaced with their neural systems over physiologically relevant timescales. The set of molecules relevant to this process are, however, not present in the structure we have studied.

## 2. MATERIAL AND METHODS

The first challenge was visualization and manipulation onto the test platform of an isolated collagen fibril whose thickness is generally less than the wavelength of visible light. Most biological materials have mechanical properties strongly dependent on their hydration state; the water in collagen fibrils acts as a platicizer (Tseretely & Smirnova 1992). Thus, our interest in testing fibrils in their hydrated state disqualified the use of an electron microscope's vacuum chamber during the loading procedure. Instead, we labelled the fibrils[2] with fluorescently tagged antibodies.[3] This procedure

[1]Stiffness was calculated using large deformation finite element analysis with the tether beams modelled as guided cantilevers.

[2]Fibrils were transported via overnight courier on wet ice. They arrived in deionized water with a small amount of azide to prevent bacterial growth. Once in our lab, the fibrils were stored at 4° C in the solution in which they were shipped.

[3]Fibrils were diluted in filtered water and labelled with a polyclonal primary goat anti-human type I collagen, Santa Cruz Biotechnology, Inc (Collagen Type I, L-19) and an Alexaflouor 568 tagged donkey anti-goat IgG from Molecular Probes.

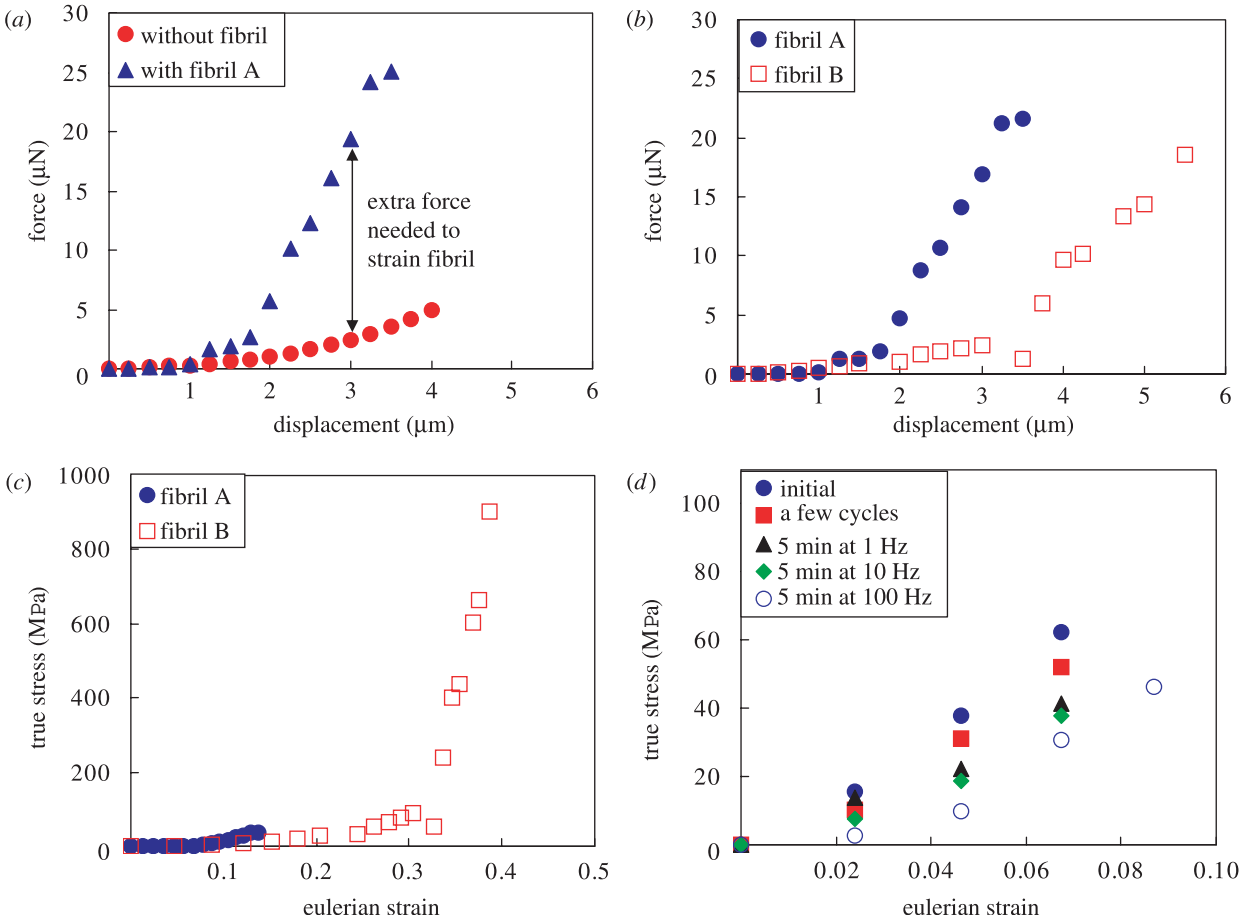


Figure 2. Mechanical response of axially loaded fibrils. (*a*) Load–displacement responses of device with and without the fibril. Subtracting the device stiffness (indicated by double arrow) provides the stiffness of the fibril. (*b*) Load–displacement curves of two fibrils with widely differing gauge lengths (fibril A = 20 μm, fibril B = 5 μm) and cross-sectional areas. (*c*) The data in (*b*) converted to true stress and Eulerian strain using SEM images from two different angles to determine cross sectional dimensions. (*d*) Stress–strain curve of a fibril measured before and after cycling under the specified conditions. Stiffness decreased upon repeated schedules of cyclic loading with measured moduli of: 0.93 GPa (initial), 0.78 GPa (few cycles), 0.59 GPa (5 min at 1 Hz), 0.55 GPa (5 min at 10 Hz), and 0.55 GPa (5 min at 100 Hz).

provides punctate staining (figure 1*d*) concomitantly allowing the possibility of measuring the strain distribution along the fibril. Using a pulled glass micropipette tip attached to a micromanipulator, the fibril is extracted from a drop of water, placed between the two pads of the micro-device, and attached to the pads using small drops of epoxy.[4] The epoxy was allowed to set for several hours with the sample maintained near the dew point. An SEM image of a fibril fixed to the testing platform is shown in figure 1*b*.

## 3. RESULTS

Figure 2*a* shows the typical force–displacement response of the device with and without the fibril labelled A. Force–displacement curves were calculated by subtracting the response of the device without a fibril from that of the device with a fibril (as shown in figure 2*b* for fibrils labelled A and B). Nominal values of secant elastic moduli at small and large strains were estimated by converting load–displacement to true stress (force divided by instantaneous area)—Eulerian (Almansi) strain. In terms of the current length, $l$, and the measured change in length, $\Delta l$, the Eulerian strain is defined as $\varepsilon = (\Delta l/l)(1-(\Delta l/2l))$. This is but one set of work-conjugate stress–strain measures available for large strain problems, and it is important to note that it is to these measures that the secant elastic moduli presented next are associated. We have not yet made any attempt to develop a phenomenological constitutive equation for the fibril. To account for the variation in cross-sectional area along the length of the fibril (Trotter *et al.* 1994) in the analysis, SEM images were collected after tensile testing. The fibrils may have shrunk as they dried (Leikin *et al.* 1997), so that the imaged fibrils are possibly thinner than they were during testing. This would result in overestimation of the elastic moduli. The cross-sections ranged from 0.43 to 1.3 $\mu m^2$, with an average of 0.71 $\mu m^2$ for fibril A, and from 0.014 to 0.12 $\mu m^2$, with an average of 0.043 $\mu m^2$ for fibril B. The instantaneous area, which we cannot yet measure during testing, was calculated under the assumption that the fibrils maintained

[4]Several adhesives were tried. The best result was obtained using 8625-S; JB Weld Co., UK.

constant volume as they stretched,[5] producing the true stress–Eulerian strain curves shown in figure 2*c*. At low strains (0.05–0.3), Fibrils A and B display similar secant elastic moduli, estimated as 0.5 and 0.4 GPa, respectively. Since fibril B is much thinner than fibril A, it achieved a greater strain. This revealed considerable stiffening in the region above 0.3 strain, as evidenced by a high strain elastic modulus of 12 GPa. The moduli measured at the lower and larger strains lie between the reported modulus of a fibre (54 MPa) (Miyazaki & Kozaburo 1999) (an ordered aggregate *ca* 1 um in diameter consisting of several hundred to several thousand fibrils) and a single collagen molecule (3–9 GPa) (Sasaki & Odajima 1996). To underscore how the values of tangent elastic moduli depend on the choice of work-conjugate stress–strain measures, we calculated (not shown in figure 2*c*) them using true stress and instantaneous strain, and obtained values of 0.4–0.3 GPa at low strains and 6 GPa at high strains.

The qualitative shape of these curves is very similar to that seen when measuring whole tendon and ligament. The toe region in these tissues is generally attributed to a kink region in the super-fibrillar structures of these tissues. There is no evidence that this structure exists in single fibrils. One previous study shows isolated fibrils loaded using an AFM (Graham *et al.* 2004). These authors focused on the stick/slip behaviour they found. However, when they used population averages to obtain cross-sectional areas and then calculated an average stress–strain curve for their data, they found a toe region. Interestingly, the toe region was also reported in load–deformation curves of single collagen molecules (Bozec & Horton 2005). The low strain portion of these single molecule measurements was well fit by a worm-like chain model. Such a model did not fit our data. We are currently investigating this issue further.

This first generation device is limited to applied loads insufficient to break the fibril, and therefore we have not determined the fibril strength. We are in the process of modifying the testing platform's geometry which will enable us to report the fibril's failure stress and strain measured from a statistically significant number of fibrils. Remarkably, these preliminary true stress–Eulerian strain curves suggest a tensile strength of the fibrils that may be greater than 1.0 GPa (corresponding to a nominal stress of 0.7 GPa).

An advantage of the electrostatic actuator is that specimens can be fatigued by cyclic loading superimposed on a mean stress by adding an ac voltage to a dc bias used to actuate the comb drive (Kahn *et al.* 2002). Figure 2*d* demonstrates our ability to perform cyclic loading of a fibril over a range of frequencies. Cycling up to the resonant frequency of the device is possible. For this fibril, the initial gauge length was 10 μm, and the cross-section ranged from 0.37 to 1.4 $\mu m^2$, with an average of 0.91 $\mu m^2$. The data show that cycling for progressively larger numbers of cycles at successively higher rates caused a monotonic decrease in the modulus of the fibril, indicating that even this small substructure is susceptible to fatigue.

Elastic moduli can also be estimated by measuring the device's resonant frequency without (8.52 kHz) and with (51.5 kHz) the fibril. Using a single degree of freedom spring-mass model, the elastic modulus of the fibril tested in figure 2*d* was determined to be 0.53 GPa, a value in good agreement with the one obtained from the stress–strain curve after all the cyclic loading was finished.

[5]The (instantaneous) cross-sectional area associated with a given displacement (and force) is calculated using the measured areas of the unloaded fiber together with the constant volume assumption. The true stress along the fiber is defined as the force divided by the instantaneous area. The stress–strain plots represent the average value of the true stress.

## 4. SUMMARY

We have demonstrated that MEMS technology offers great promise to measure the mechanical properties of single nanofibrils under ambient conditions. The device we used is associated with relatively 'clean' tension boundary conditions. Use of optically fluorescent markers allows for precise reproducible manipulation of the fibrils and avoids the dehydrating vacuum of an SEM. We expect the combination of these benefits will allow investigators to move forward in their measurement and analysis of soft nanofibrils in a manner heretofore impossible. Furthermore, with minor modifications the MEMS platform can provide a wide range of forces and displacements useful to measure the properties of other nanoscale fibres and membrane structures (carbon nanotubes, cell membranes).

Research supported by the National Science Foundation (grant no. 0403876) and the National Institutes of Health (grant no. 1 R21 EB004985-01A1). We thank Prof. John Trotter of the University of New Mexico for gifting the fibrils, Dr Li Chen of Case for performing the finite element analyses of the tether beams and Prof. Arthur Heuer of Case for suggesting use of adhesives to fix fibrils to the device.

## REFERENCES

Ashby, M. F., Gibson, L. J., Wegst, U. & Olive, R. 1995 The mechanical-properties of natural materials. 1. Material property charts. *Proc. R. Soc. A* **450**, 123–140.

Baer, E., Hiltner, A. & Keith, H. D. 1987 Hierarchical structure in polymeric materials. *Science* **235**, 1015–1022.

Best, R. B., Li, B., Steward, A., Daggett, V. & Clarke, J. 2001 Can non-mechanical proteins withstand force? Stretching barnase by atomic force microscopy and molecular dynamics simulation. *Biophys. J.* **81**, 2344–2356.

Bozec, L. & Horton, M. 2005 Topography and mechanical properties of single molecules of type I collagen using atomic force microscopy. *Biophys. J.* **88**, 4223–4231. (doi:10.1529/biophysj.104.055228)

Bryant, Z. *et al.* 2003 Structural transitions and elasticity from torque measurements on DNA. *Nature* **424**, 338–341. (doi:10.1038/nature01810)

Butler, E., Hardin, J. & Benson, S. 1987 The role of lysyl oxidase and collagen crosslinking during sea urchin development. *Exp. Cell Res.* **173**, 174–182. (doi:10.1016/0014-4827(87)90343-0)

Clausen-Schaumann, H., Rief, M., Tolksdorf, C. & Gaub, H. E. 2000 Mechanical stability of single DNA molecules. *Biophys. J.* **78**, 1997–2007.

Fujii, T., Sun, Y. L., An, K. N. & Luo, Z. P. 2002 Mechanical properties of single hyaluronan molecules. *J. Biomech.* **35**, 527–531. (doi:10.1016/S0021-9290(01)00205-6)

Graham, H. K., Holmes, D. F., Watson, R. B. & Kadler, K. E. 2000 Identification of collagen fibril fusion during vertebrate tendon morphogenesis. The process relies on unipolar fibrils and is regulated by collagen-proteoglycan interaction. *J. Mol. Biol.* **295**, 891–902. (doi:10.1006/jmbi.1999.3384)

Graham, J. S., Vomund, A. N., Phillips, C. L. & Grandbois, M. 2004 Structural changes in human type I collagen fibrils investigated by force spectroscopy. *Exp. Cell Res.* **299**, 335–342. (doi:10.1016/j.yexcr.2004.05.022)

Heim, L. O., Kappl, M. & Butt, H. J. 2004 Tilt of atomic force microscope cantilevers: effect on spring constant and adhesion measurements. *Langmuir* **20**, 2760–2764. (doi:10.1021/la036128m)

Kahn, H., Ballarini, R., Mullen, R. L. & Heuer, A. H. 1999 Electrostatically actuated failure of microfabricated polysilicon fracture mechanics specimens. *Proc. R. Soc. A* **455**, 3807–3823. (doi:10.1098/rspa.1999.0478)

Kahn, H., Ballarini, R., Bellante, J. J. & Heuer, A. H. 2002 Fatigue failure in polysilicon not due to simple stress corrosion cracking. *Science* **298**, 1215–1218.

Kamat, S., Su, X., Ballarini, R. & Heuer, A. H. 2000 Structural basis for the fracture toughness of the shell of the conch Strombus gigas. *Nature* **405**, 1036–1040. (doi:10.1038/35016535)

Kastelic, J., Galeski, A. & Baer, E. 1978 The multicomposite structure of tendon. *Connect Tissue Res.* **6**, 11–23.

Kellermayer, M. S., Smith, S. B., Bustamante, C. & Granzier, H. L. 2001 Mechanical fatigue in repetitively stretched single molecules of titin. *Biophys. J.* **80**, 852–863.

Lakes, R. 1993 Materials with structural hierarchy. *Nature* **361**, 511–515. (doi:10.1038/361511a0)

Leikin, S., Parsegian, V. A., Yang, W. & Walrafen, G. E. 1997 Raman spectral evidence for hydration forces between collagen triple helices. *Proc. Natl Acad. Sci. USA* **94**, 11312–11317. (doi:10.1073/pnas.94.21.11312)

Liphardt, J., Onoa, B., Smith, S. B., Tinoco, I. & Bustamante, C. 2001 Reversible unfolding of single RNA molecules by mechanical force. *Science* **292**, 733–737. (doi:10.1126/science.1058498)

Mehta, A. D., Rief, M., Spudich, J. A., Smith, D. A. & Simmons, R. M. 1999 Single-molecule biomechanics with optical methods. *Science* **283**, 1689–1695. (doi:10.1126/science.283.5408.1689)

Miyazaki, H. & Kozaburo, H. 1999 Tensile tests of collagen fibers obtained from the rabbit patellar tendon. *Biomed. Microdevices* **2**, 151–157. (doi:10.1023/A:1009953805658)

Muller, D. J. *et al.* 2002 Stability of bacteriorhodopsin alpha-helices and loops analyzed by single-molecule force spectroscopy. *Biophys. J.* **83**, 3578–3588.

Rainey, J. K., Wen, C. K. & Goh, M. C. 2002 Hierarchical assembly and the onset of banding in fibrous long spacing collagen revealed by atomic force microscopy. *Matrix Biol.* **21**, 647–660. (doi:10.1016/S0945-053X(02)00101-4)

Rho, J. Y., Kuhn-Spearing, L. & Zioupos, P. 1998 Mechanical properties and the hierarchical structure of bone. *Med. Eng. Phys.* **20**, 92–102. (doi:10.1016/S1350-4533(98)00007-1)

Sasaki, N. & Odajima, S. 1996 Stress–strain curve and Young's modulus of a collagen molecule as determined by the X-ray diffraction technique. *J. Biomech.* **29**, 655–658. (doi:10.1016/0021-9290(95)00110-7)

Thurmond, F. & Trotter, J. 1996 Morphology and biomechanics of the microfibrillar network of sea cucumber dermis. *J. Exp. Biol.* **199**, 1817–1828.

Trotter, J. A., Thurmond, F. A. & Koob, T. J. 1994 Molecular-structure and functional-morphology of echinoderm collagen fibrils. *Cell Tissue Res.* **275**, 451–458. (doi:10.1007/BF00318814)

Tseretely, G. I. & Smirnova, O. I. 1992 DSC study of melting and glass-transition in gelatins. *J. Thermal. Anal.* **38**, 1189–1201. (doi:10.1007/BF01979179)

Veigel, C., Bartoo, M. L., White, D. C., Sparrow, J. C. & Molloy, J. E. 1998 The stiffness of rabbit skeletal actomyosin cross-bridges determined with an optical tweezers transducer. *Biophys. J.* **75**, 1424–1438.

Yu, M. F. *et al.* 2000 Strength and breaking mechanism of multiwalled carbon nanotubes under tensile load. *Science* **287**, 637–640. (doi:10.1126/science.287.5453.637)